Research Article Vol. 12, No. 11 / November 2024 / Photonics Research 2573

PHOTONICS Research

Maximizing transmission capacity in optical communication systems utilizing a microresonator comb laser source with adaptive modulation and bandwidth allocation strategies

Jun Hu,[1,2,†] Wei Wang,[3,4,†] Zhenyu Xie,[5,†] Chengnian Liu,[1,2] Fan Li,[3,4,6] and Daquan Yang[1,2,7]

[1]State Key Laboratory of Information Photonics and Optical Communications, Beijing University of Posts and Telecommunications, Beijing 100876, China
[2]School of Information and Communication Engineering, Beijing University of Posts and Telecommunications, Beijing 100876, China
[3]School of Electronics and Information Technology, Sun Yat-sen University, Guangzhou 510275, China
[4]Key Laboratory of Optoelectronic Materials and Technologies, School of Electronics and Information Technology, Sun Yat-sen University, Guangzhou 510275, China
[5]State Key Laboratory for Artificial Microstructure and Mesoscopic Physics and Frontiers Science Center for Nano-optoelectronics, School of Physics, Peking University, Beijing 100871, China
[6]e-mail: lifan39@mail.sysu.edu.cn
[7]e-mail: ydq@bupt.edu.cn
[†]These authors contributed equally to this work.

Received 20 June 2024; revised 23 July 2024; accepted 23 August 2024; posted 23 August 2024 (Doc. ID 533500); published 31 October 2024

Traditional optical communication systems employ bulky laser arrays that lack coherence and are prone to severe frequency drift. Dissipative Kerr soliton microcombs offer numerous evenly spaced optical carriers with a high optical signal-to-noise ratio (OSNR) and coherence in chip-scale packages, potentially addressing the limitations of traditional wavelength division multiplexing (WDM) sources. However, soliton microcombs exhibit inhomogeneous OSNR and linewidth distributions across the spectra, leading to variable communication performance under uniform modulation schemes. Here, we demonstrate, for the first time, to our knowledge, the application of adaptive modulation and bandwidth allocation strategies in optical frequency comb (OFC) communication systems to optimize modulation schemes based on OSNR, linewidth, and channel bandwidth, thereby maximizing capacity. Experimental verification demonstrates that the method enhances spectral efficiency from 1.6 to 2.31 bit $\cdot s^{-1} \cdot Hz^{-1}$, signifying a 44.58% augmentation. Using a single-soliton microcomb as the light source, we achieve a maximum communication capacity of 10.68 Tbps after 40 km of transmission in the C-band, with the maximum single-channel capacity reaching 432 Gbps. The projected combined transmission capacity for the C- and L-bands could surpass 20 Tbps. The proposed strategies demonstrate promising potential of utilizing soliton microcombs as future light sources in next-generation optical communication.

https://doi.org/10.1364/PRJ.533500

1. INTRODUCTION

On the verge of an information explosion, driven by the exponential growth of cloud applications and Internet traffic, ultra-high speed and capacity are demanded in optical fiber communications. Massively parallel wavelength division multiplexing (WDM) is deemed crucial for achieving ultra-high capacity in optical communications [1–6]. However, conventional commercial WDM systems, requiring tens or hundreds of lasers to provide optical carriers, significantly impact the size, cost, and power consumption of the system negatively [7–9]. The need for higher coherence and frequency stability of the carrier laser increases with narrower channel spacing and higher data rates [10–12]. Practically, WDM systems require widened guard bands to prevent spectral overlap due to laser frequency offsets, which restricts the system's capacity from reaching the Shannon limit. Additionally, since the laser linewidth affects the phase noise of the signal, a broader linewidth results in greater phase fluctuations. These phase fluctuations cause demodulation errors, thereby degrading the performance of the transmission system, especially in higher-order modulation schemes [13]. However, the linewidths of integrated tunable laser arrays (ITLAs) in conventional WDM systems, typically several hundred kHz, restrict their use in advanced modulation formats. A viable solution to this challenge is the adoption of optical frequency combs (OFCs) [14]. By pumping a whispering-gallery-mode (WGM) microresonator with a continuous-wave

laser, numerous OFCs with high-frequency stability and ultralow phase noise can be produced. Many types of resonators, including microring [15,16], microdisk [17], and microsphere resonators [18], are capable of generating OFC.

Silicon nitride (Si_3N_4) microring resonators, compared to other types, offer a more mature process for generating broadband and fully phase-coherent time-dissipative Kerr solitons (DKSs), presenting significant potential as on-chip optical frequency comb generators. Recently, OFCs have found extensive applications in fields like sensing [19–22], timekeeping [23,24], spectroscopy [25], precision metrology [26,27], and optical communications [28–33]. In optical communications, OFCs have achieved significant advancements in capacity [30] and digital signal processing (DSP) simplification [31]. However, as predetermined by the solution to the Lugiato-Lefever equation and the effect of repetition rate fluctuations, the optical signal-to-noise ratios (OSNRs) and linewidths of the soliton microcombs are not uniformly distributed [34,35]. Therefore, using one fixed modulation scheme will inevitably fail to effectively utilize the full bandwidth potential of soliton microcombs. Among the conventional communication algorithms [36,37], adaptive modulation and bandwidth allocation strategies stand out as promising solutions. Adaptive modulation dynamically adjusts the modulation scheme by continuously monitoring the channel state information (CSI), selecting the modulation that best suits the current environment to optimize the data transmission rate and reliability. Bandwidth allocation strategies dynamically distribute bandwidth resources in a communication network and adjust bandwidth in real time based on changes in network traffic to improve resource utilization.

Here, we introduce the use of adaptive modulation and bandwidth allocation strategies for the first time in high-capacity OFC communication experiments. Unlike conventional communication systems that dynamically adjust based on CSI and user resources, this study applies strategies to optimize symbol rates and modulation formats for comb lines with varying carrier qualities (e.g., OSNR, linewidth), to enhance spectral efficiency and communication quality. For comb lines with lower communication performance, in this paper, the unused bandwidth in the channel is effectively utilized by converting the bandwidth space in the frequency domain to the phase space in the constellation diagram, using a low-order modulation format and a high-speed symbol transmission rate. This approach results in a 44.58% improvement in spectral efficiency. In addition, the adaptive modulation and bandwidth allocation strategy optimizes the system communication capacity based on OFC quality and system resources. Therefore, it is applicable to all OFC communication systems. With this method, we experimentally measure the capacity limit of each channel in a single-soliton microcomb generated by a Si_3N_4 microring resonator. The system utilizes 39 optical combs in the C-band, achieving a total transmission capacity of 10.68 Tbps over a distance of 40 km, with a maximum single-channel capacity of 432 Gbps. This exceeds the single-channel capacity of the next-generation commercial WDM system of 400 Gbps. Additionally, we present the experimentally measured single-sideband (SSB) frequency noise for each channel of the soliton microcomb. The frequency noise is minimal near the pump light and increases continuously toward both ends, with the minimum measured frequency noise being 17.56 Hz^2/Hz, equivalent to a Lorentzian linewidth of 107 Hz. The experimental results demonstrate that the communication quality of different comb lines in a soliton microcomb mainly depends on the OSNR and linewidth of individual comb lines. The communication capacity of the soliton microcomb can be maximized by using adaptive modulation algorithms and bandwidth allocation strategies dynamically adjusted according to the conditions of each channel.

2. GENERATION AND CHARACTERIZATION OF THE SINGLE-SOLITON MICROCOMB

Before conducting the soliton microcomb communication experiments to verify the effects of adaptive modulation and bandwidth allocation strategies, we first measure the OSNR and linewidth of the soliton microcomb. Figure 1(a) illustrates the experimental setup used to generate a soliton microcomb in a high-Q Si_3N_4 microring resonator. This setup facilitates the generation of a stable soliton microcomb using minimal instrumentation and straightforward operation, maintaining stability for over 10 h. In coherent optical communications, the Lorentz linewidth is critical as it controls the instantaneous frequency and phase fluctuations over short time scales, requiring precise tracking by receivers to effectively compensate for distortion. Dissipative solitons demonstrate low-noise coherent states, with the ideal scenario being that the frequency noise of the soliton microcomb is primarily derived from the pump laser's frequency noise. Consequently, an ultra-narrow linewidth fiber laser is used as the pump source. While lower-power pump light can generate a stable soliton microcomb, amplifying the narrow linewidth laser to about 26 dBm using an erbium-doped fiber amplifier (EDFA) optimizes the OSNR of the carrier. However, the amplified spontaneous emission (ASE) noise from the EDFA reduces the OSNR of carriers near the pump light, requiring a narrowband bandpass filter post-EDFA to mitigate ASE noise. Optimal optical power distribution occurs when the polarization of the continuous-wave (CW) pump laser aligns with its polarization axis. To achieve this, polarization controllers are used to adjust the polarization state. A fiber Bragg grating (FBG) is employed for post-packaging of the Si_3N_4 microresonator to suppress the residual pump light.

The transmission power spectrum is recorded by a photodetector and monitored by an oscilloscope, while the soliton spectrum is monitored by a spectrometer. Figure 1(b) displays a microscope photo of the packaged Si_3N_4 microring resonator used for communication experiments, with a free spectral range (FSR) of approximately 100.58 GHz and enclosed with a temperature sensing control module for temperature stabilization. Figure 1(c) shows the Q factor of the Si_3N_4 microring resonator with an intrinsic Q of 1.082×10^7. To assess the long-term stability of the sensing system, the shifts of the resonance wavelength with and without temperature control are measured over time. The resonant frequency shift with temperature control, as shown in Fig. 1(d), is suppressed by an order of magnitude to mere 0.46 pm, indicating outstanding stability of the packaging. Additionally, the generated soliton microcomb can also be maintained for more than 10 h, showing great potential in long-term operation.

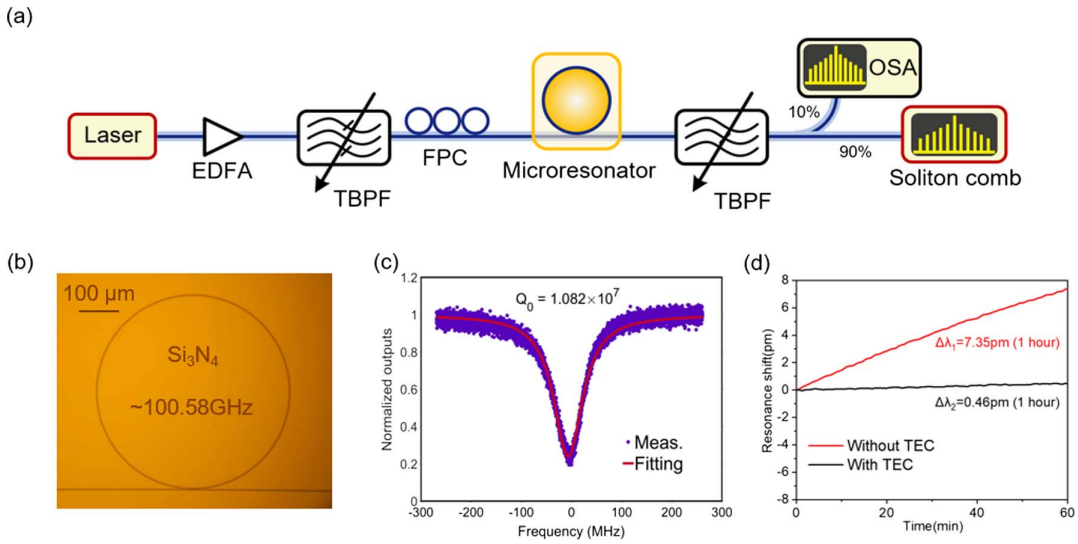

Fig. 1. (a) Experimental setup for generating a single-soliton microcomb in a high-Q Si_3N_4 microring resonator. EDFA: erbium-doped fiber amplifier; TBPF: tunable bandpass filter; FPC: fiber polarization controller; OSA: optical spectrum analyzer. (b) Microscope photo of a Si_3N_4 microring resonator with a radius of about 240 μm. (c) Typical transmission spectrum and Q-factor of the resonator resonance mode. (d) Variation of 1 h resonance wavelength with and without temperature control.

After suppressing the residual pump light, the measured spectrum of the single-soliton microcomb is shown in Fig. 2(a), exhibiting a smooth spectrum profile with a 3 dB bandwidth of 6 THz. The soliton microcomb features a broad spectrum in the frequency domain, which generates ultra-high-power pulsed signals in the time domain. Meticulous power management is crucial to protect the in-phase and quadrature modulator (IQM) from potential damage caused by excessive comb power. Additionally, since C-band fiber has the lowest transmission loss and is the most commonly used band in WDM systems, which are widely used in metropolitan area networks (MANs), long-haul, ultra-long-haul, and submarine fiber cable systems, our experiments also focus on the C-band region. Figure 2(b) shows the spectra of the soliton microcomb within the C-band region. A 10 dB difference in comb line power can be observed, which would affect the communication bandwidth if not addressed.

In addition, different communication modulation formats have different linewidth requirements for the optical carrier. In conventional communication systems, higher-order modulation formats increase the bandwidth for a given modulation rate, but require lower phase noise in the carrier to maximize constellation density in phase space. Employing an ultralow-noise pump laser allows the soliton microcomb to achieve extremely narrow linewidths. The gain of the soliton microcomb is based on resonantly enhanced continuous-wave pump

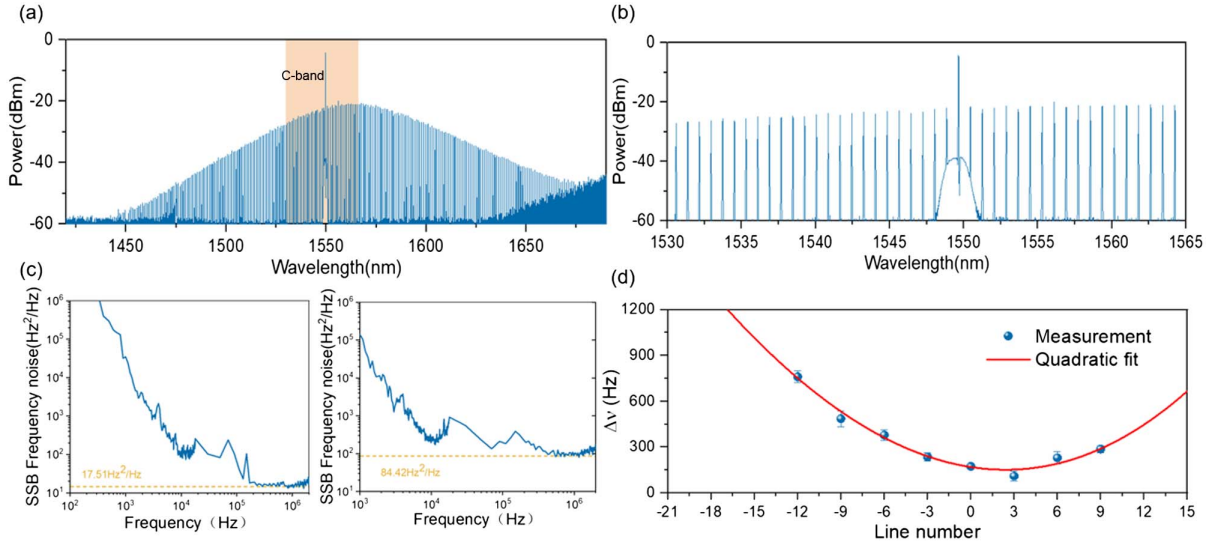

Fig. 2. (a) Optical spectra of the single-soliton microcomb. (b) C-band spectra of the single-soliton microcomb before modulation. (c) Respective SSB frequency noise spectra of the 1552 and 1542.4 nm comb line. (d) Distribution of the soliton microcomb linewidth. The error bar stands for the standard deviation of three measurements.

parametric amplification, with noise induced by spontaneous scattering being extremely weak. Within the microcomb, the pump laser is coherently integrated into the comb-like spectrum, resulting in its noise being expected to be equally transferred to all comb lines. Previous studies have indicated that when the microcomb operates with low noise, the comb lines inherit the linewidth of the pump, and farther lines attenuate more due to repetition noise within the cavity [35,38].

The linewidth and OSNR of optical combs in coherent communication systems affect the communication capability of the system jointly. Here, a delayed self-heterodyne interference (DSHI) scheme is utilized [39] to measure the distribution of the soliton microcomb frequency noise. This method utilizes a laser to generate two light beams with different delays for self-heterodyning and exploits the spectral characteristics of self-heterodyning to measure comb line linewidth. A wavelength selective switch (WaveShaper) is utilized to filter out individual comb lines from the soliton microcomb into the DSHI setup. The comb line is split into two paths through a beam splitter, with one path passing through an acoustic optical modulator (AOM) for frequency shifting and the other path through a 10-km-long optical fiber delay line. They are then mixed in a photodetector to generate a beatnote containing the phase fluctuation of the comb line. Figure 2(c) shows the single-sideband (SSB) frequency noise spectra measured at the 1552 nm comb line and the 1542.4 nm comb line, with white noise floors at 17.51 Hz^2/Hz and 84.42 Hz^2/Hz, respectively. Taking into account the relationship between frequency noise (S_ν) and the fundamental linewidth ($\Delta\nu S_T$) ($\Delta\nu S_T = 2\pi S_\nu$), the Lorentzian linewidth of the 1552 nm comb line can be calculated as 107 Hz. The linewidths of the respective comb lines from $m = -21$ to $m = 15$ are shown in Fig. 2(d), following a quadratic pattern as projected by repetition noise [35]. A noise degradation of more than two orders of magnitude can be observed in marginal comb lines, which can impact the communication performance under conventional modulation schemes. Despite that, experimental results indicate that the linewidth of the integrated microcavity OFC is about three orders of magnitude smaller than the linewidth of the ITLA laser array used in commercial WDM systems [40]. This substantial reduction in linewidth is highly advantageous for long-distance transmission and the implementation of higher-order modulation formats.

3. HIGH-CAPACITY COMMUNICATION SYSTEM BASED ON THE SINGLE-SOLITON MICROCOMB

A. Experimental Setup

After generating a single-soliton microcomb using an integrated microcavity, we construct an OFC coherent communication system to simulate a realistic WDM coherent optical communication scenario. The experimental setup shown in Fig. 3 is used to assess the communication capability of each comb tooth in the soliton microcomb, which implements adaptive modulation and bandwidth allocation strategies. To simulate typical WDM communication transmission scenarios, the OFC is divided into odd and even carrier groups using a WDM multiplexer. A C-band programmable filter (Finisar WaveShaper) is used to function as the WDM multiplexer. Following this, each set of odd and even carriers is amplified separately using polarization-maintaining EDFAs before being modulated by two IQMs. Since only one DP-IQM is available, the amplified even optical carriers are injected into an IQM for modulation. To simulate the dual-polarization modulation, the output of the modulator is divided into two branches by an optical coupler (OC), with both branches theoretically having equal power. As shown in Fig. 3, to achieve de-correlation between the two branches, a delay line of about 1 m is added to the lower branch in order to introduce an appropriate time delay. This delay ensures that the two channels are sufficiently differentiated to form a doubly polarized signal when merged via the OC.

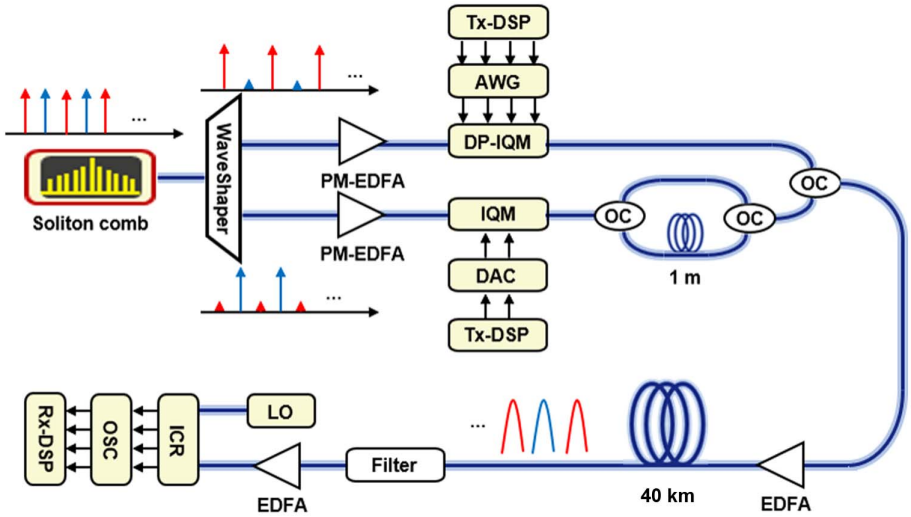

Fig. 3. Experimental setup for soliton microcomb coherent communication. WaveShaper: waveform shaper; Tx-DSP: data signal processing sender port; AWG: arbitrary waveform generator; DAC: digital to analog converter; DP-IQM: dual polarization IQM; OC: optical coupler; Fiber: 40 km of single-mode fiber; PM-EDFA: bias-preserving erbium-doped fiber amplifier; Filter: narrowband optical filter; ICR: coherent optical receiver; OSC: real-time oscilloscope; Rx-DSP: data signal processing receiver port; and LO: local oscillator.

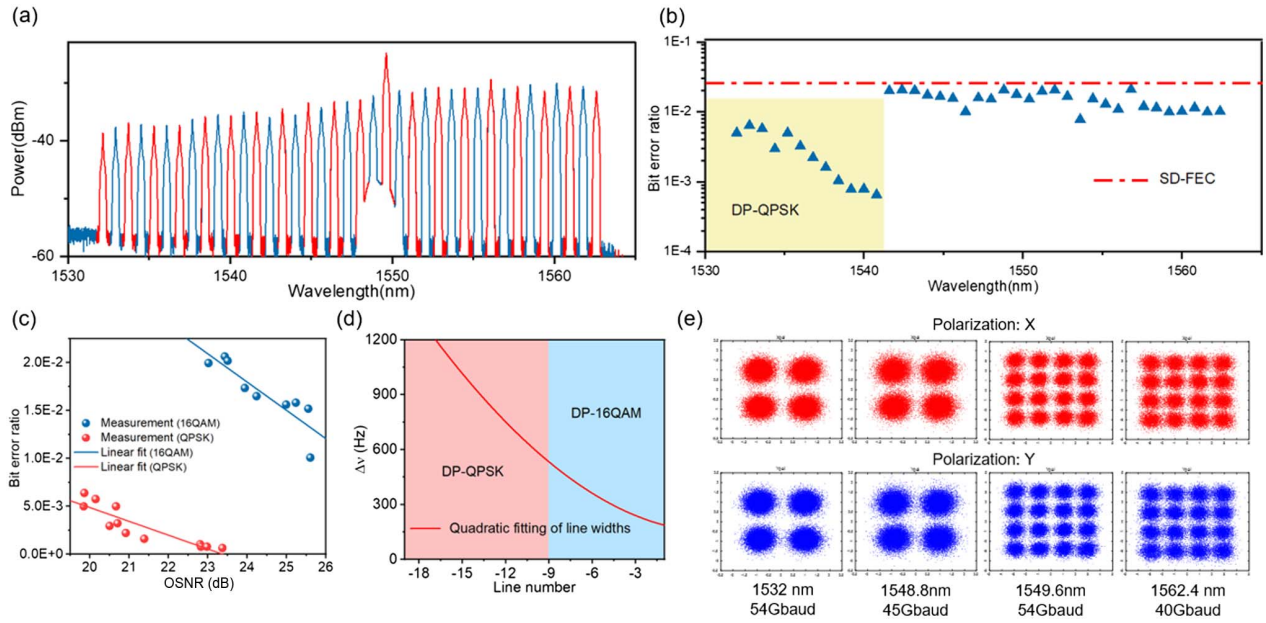

Fig. 4. (a) Optical spectra of 39 channels modulated with 40 Gbaud and DP-16QAM modulation format (measured at OC). The red and blue colors of the carriers represent the parity carriers. (b) Measured bit error ratios of the transmitted channels for the single comb with a received power of −14 dBm and a modulation symbol transmission rate of 40 Gbaud. The red dashed line indicates the soft decision forward error correction (SD-FEC) BER threshold with an overhead of 20%. The 12 lines at the high-frequency edge of the C-band (yellow region) are modulated with quadrature phase-shift keying (QPSK) signals rather than 16QAM owing to the large linewidths of these carriers. (c) Measured bit error ratios versus combs OSNR for QPSK modulated channels and neighboring 16QAM modulated channels. (d) Linewidth distribution of the corresponding channel in (c), and the powder blue background represents the modulation formats DP-QPSK and DP-16QAM used by the carriers in range. (e) Constellation diagrams of soliton coherent communication obtained at carrier wavelengths of 1532, 1548.8, 1549.6, and 1562.4 nm at a received power of −14 dBm.

After modulating the odd and even carriers, the signals are combined using an OC combiner, and Fig. 4(a) depicts the spectrum of the resultant signal. Prior to transmission through a 40 km single-mode fiber, the modulated signal is further amplified by an EDFA. At the receiver end, the signal is filtered through a narrowband optical filter with a bandwidth of 75 GHz. The filtered single-channel signal is then directed to the coherent receiver for demodulation by the local oscillator (LO) and captured by the real-time oscilloscope (OSC). The drive signals for the DP-IQM and the IQM are generated by a four-channel arbitrary waveform generator (AWG) at 64 GS/s and a two-channel digital-to-analog converter (DAC) at 80 GS/s, respectively. Importantly, the bias point of the Mach–Zehnder modulator (MZM) is deliberately adjusted closer to its null point to reduce optical fluctuations in the waveform's lower region. For modulation, quadrature phase shift keying (QPSK) or 16-quadrature amplitude modulation (16QAM) formats are used, combined with cosine-shaped raised pulse shaping, with a roll-off factor (β) at 0.1.

B. Experimental Results

Due to the strong attenuation of the C-band waveform shaper at the edge of the band, modulation and capacity measurements are performed only on 39 optical combs with wavelengths ranging from 1532 to 1562.4 nm at a wavelength spacing of approximately 0.8 nm, as determined by the comb FSR. Figure 4(a) displays the optical spectra of the 39 modulated optical combs using 40 Gbaud 16QAM signals. Notably, due to the low OSNR and large frequency noise of the 12 combs in the C-band soliton microcombs with wavelengths lower than 1541.6 nm, error-free transmission is not possible using 40 Gbaud and 16QAM, so 40 Gbaud and QPSK modulation are used to measure the BER. The BER of each channel after demodulation is shown in Fig. 4(b). The results reveal significant variations in communication capabilities among different combs of the same soliton microcomb. If the same modulation format and symbol rate are used across all combs, the overall communication performance is limited by the poorest-performing comb, known as the "barrel effect". Therefore, selecting an appropriate modulation scheme for each comb line is crucial for microcomb-based communication.

To more accurately and reliably investigate the relationship between the communication performance of soliton microcombs and OSNR, the data of the three comb lines that are affected by the ASE noise from the EDFA are ignored, retaining only the data of the pump light with the same baseline noise. The blue dots in Fig. 4(c) are the relationship between BER and OSNR for the nine channels from 1541.6 to 1548 nm with 40 Gbaud 16QAM, while red dots are the 12 channels from 1532 to 1540.8 nm using the 40 Gbaud QPSK. The experimental results for both modulation formats show that the BER increases with the decrease of the OSNR, causing the degradation of the communication performance. Although increasing the optical pump power can improve the OSNR of the soliton microcombs and enhance overall

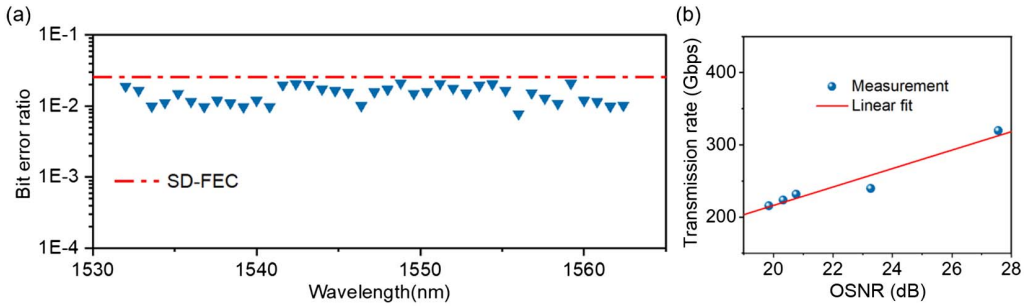

Fig. 5. (a) Measured bit error ratios of the transmitted channels for each channel at the maximum transmission rate with a received power of −14 dBm. The red dashed line indicates the soft decision forward error correction (SD-FEC) BER threshold with an overhead of 20%. (b) Measured single-wave maximum rate versus OFC OSNR.

communication performance, this approach is power consuming and does not address the uneven OSNR distribution of the soliton microcombs fundamentally. It is noteworthy that the six channels from 1539.2 to 1543.2 nm have similar OSNRs, yet the three channels from 1539.2 to 1540.8 nm cannot achieve error-free transmission with the 40 Gbaud 16QAM as effectively as the channels from 1541.6 to 1543.2 nm. This indicates that OSNR is not the sole factor influencing OFC communication performance. The increasing linewidth of the comb lines from 1543.2 to 1539.2 nm, as shown in Fig. 4(d), reduces constellation density in phase space, leading to constellation aliasing and higher BERs. Figure 4(e) shows the constellation diagrams for the 1532 nm channel (leftmost C-band), the 1548.8 nm channel with QPSK modulation due to ASE noise, the 1549.6 nm channel (pumped light), and the 1562.4 nm channel (rightmost C-band). These diagrams illustrate the significant impact of ASE noise on communication performance. Despite channel 1548.8 nm having a lower capacity than channel 1532 nm, its constellation diagrams are blurrier. The constellation diagrams indicate good communication performance across all channels. As shown in Fig. 4(b), we observe that the comb line to the left of the pump light (i.e., those with shorter wavelengths than the pump light) exhibits a decreasing OSNR and an increasing linewidth as the wavelength decreases. This combination results in deteriorating communication performance for the optical combs on the left as the wavelength decreases. Conversely, the optical combs on the right side of the pump light show a more balanced communication performance due to a simultaneous increase in both OSNR and linewidth. Given these distribution characteristics, we can employ low-order modulation formats such as QPSK with higher symbol transmission rates for the comb lines on the left side of the pump light. For the comb lines on the right side, which have better communication performance, higher-order modulation formats such as 16QAM are suitable. Additionally, when designing the appropriate communication scheme for each comb line, it is essential to consider not only the OSNR and linewidth but also the channel bandwidth to avoid spectral aliasing.

To maximize the transmission rate of soliton microcombs, we employ adaptive modulation and bandwidth allocation strategies for the first time in OFC communication systems. Based on the OSNR and linewidth of different channels, the modulation format and symbol transmission rate are manually adjusted within the constraint of channel bandwidth until the BER reaches the threshold of 2.5×10^{-2} defined by the third-generation soft decision forward error correction (FEC). This approach maximizes the communication performance of the entire soliton communication system and achieves the highest spectral efficiency. Using this setup, we determine the maximum total capacity of the C-band soliton microcomb to be 10.68 Tbps for the 39 comb lines. In the wavelength range of 1532–1540.8 nm, 12 channels used the QPSK modulation format with baud rates ranging from 54 to 60 Gbaud. This method increases the spectral efficiency from $1.6\ \text{bit}\cdot\text{s}^{-1}\cdot\text{Hz}^{-1}$ in the first experiment to $2.31\ \text{bit}\cdot\text{s}^{-1}\cdot\text{Hz}^{-1}$, reflecting a 44.58% improvement, which demonstrates the method's efficacy. Figure 5(a) shows the transmission BER measurements for each channel at a received power of −14 dBm after applying the adaptive modulation and bandwidth allocation strategy, indicating that each comb line achieves near-maximum communication performance. Figure 5(b) plots the maximum communication capacity of the comb versus the OSNR of the comb, showing a clear linear relationship where higher OSNR allows for greater data capacity transmission. This result demonstrates that the original communication performance of soliton microcombs can be fully exploited using adaptive modulation and bandwidth allocation strategies. This is particularly important for combs with low OSNR and large linewidth, which are often overlooked because of their poor communication performance. Given the impending capacity crisis in optical fiber communication systems, maximizing the communication capacity of each channel is critical.

4. CONCLUSION

In summary, we have implemented adaptive modulation and bandwidth allocation strategies for the first time in a soliton microcomb communication system. This method employs the most appropriate capacity-maximizing modulation scheme for each channel, considering the constraints of channel bandwidth by detecting the OSNR and linewidth distribution of the soliton microcombs. Furthermore, the method is validated through two control experiments: the first follows the conventional fixed modulation scheme, while the second utilizes our method. Our results indicate that the adaptive modulation and bandwidth allocation strategies significantly improve the

communication performance of the soliton microcomb, particularly for the segments of the comb with initially poor communication performance. Spectral efficiency is improved from 1.6 to 2.31 bit $\cdot s^{-1} \cdot$ Hz^{-1}, representing a 44.58% improvement. We evaluate the maximum communication capacity of the soliton microcombs after 40 km of transmission, finding that the total communication capacity of the C-band exceeds 10 Tbps, with the maximum single-channel rate reaching 432 Gbps. The capacity of the C+L-band is expected to exceed 20 Tbps. Owing to the simplicity and maturity of such strategies, they are readily compatible with commercial components. Our results highlight the potential of integrated microcavity optical frequency combs as a next-generation light source for WDM communications, especially in intra/inter-data center networks where ultralow latency and cost-effectiveness are crucial.

Funding. Beijing Municipal Natural Science Foundation (Z210004); National Key Research and Development Program of China (SQ2023YFB2805600); State Key Laboratory of Information Photonics and Optical Communications, BUPT, China (IPOC2021ZT01); Beijing Nova Program from Beijing Municipal Science and Technology Commission (20230484433); Fundamental Research Funds for the Central Universities (2023PY08); Beijing University of Posts and Telecommunications (530224024); National Natural Science Foundation of China (62271517); Basic and Applied Basic Research Foundation of Guangdong Province (2023B1515020003); State Key Laboratory of Advanced Optical Communication Systems and Networks of China (2024GZKF19).

Acknowledgment. The authors thank Bing Duan, Dr. Yongpan Gao, and Dr. Huashun Wen for the helpful discussions.

Disclosures. The authors declare no conflicts of interest.

Data Availability. Data underlying the results presented in this article are not publicly available at this time, but may be obtained from the authors upon reasonable request.

REFERENCES

1. N. Froberg, S. Henion, H. Rao, *et al.*, "The NGI onramp test bed: reconfigurable WDM technology for next generation regional access networks," J. Lightwave Technol. **18**, 1697–1708 (2000).
2. E. Agrell, M. Karlsson, A. Chraplyvy, *et al.*, "Roadmap of optical communications," J. Opt. **18**, 063002 (2016).
3. S. L. Jansen, I. Morita, T. C. Schenk, *et al.*, "Coherent optical 25.8-Gb/s OFDM transmission over 4160-km SSMF," J. Lightwave Technol. **26**, 6–15 (2008).
4. S. J. Savory, "Digital coherent optical receivers: algorithms and subsystems," IEEE J. Sel. Top. Quantum Electron. **16**, 1164–1179 (2010).
5. Z. Liu, J.-Y. Kim, D. S. Wu, *et al.*, "Homodyne OFDM with optical injection locking for carrier recovery," J. Lightwave Technol. **33**, 34–41 (2014).
6. G. Rademacher, B. J. Puttnam, R. S. Luís, *et al.*, "10.66 peta-bit/s transmission over a 38-core-three-mode fiber," in *Optical Fiber Communication Conference* (Optica Publishing Group, 2020), paper Th3H-1.
7. P. J. Winzer, "Scaling optical fiber networks: challenges and solutions," Opt. Photonics News **26**, 28–35 (2015).
8. F. Hamaoka, K. Minoguchi, T. Sasai, *et al.*, "150.3-Tb/s ultra-wideband (S, C, and L bands) single-mode fibre transmission over 40-km using > 519 Gb/s/A PDM-128QAM signals," in *European Conference on Optical Communication (ECOC)* (IEEE, 2018), pp. 1–3.
9. T. Kobayashi, M. Nakamura, F. Hamaoka, *et al.*, "1-Pb/s (32 SDM/46 WDM/768 Gb/s) C-band dense SDM transmission over 205.6-km of single-mode heterogeneous multi-core fiber using 96-Gbaud PDM-16QAM channels," in *Optical Fiber Communications Conference and Exhibition (OFC)* (IEEE, 2017), pp. 1–3.
10. H. Hu, F. Da Ros, M. Pu, *et al.*, "Single-source chip-based frequency comb enabling extreme parallel data transmission," Nat. Photonics **12**, 469–473 (2018).
11. J. Schröder, A. Fülöp, M. Mazur, *et al.*, "Laser frequency combs for coherent optical communications," J. Lightwave Technol. **37**, 1663–1670 (2019).
12. S. A. Diddams, K. Vahala, and T. Udem, "Optical frequency combs: coherently uniting the electromagnetic spectrum," Science **369**, eaay3676 (2020).
13. W. Liang, D. Eliyahu, V. S. Ilchenko, *et al.*, "High spectral purity Kerr frequency comb radio frequency photonic oscillator," Nat. Commun. **6**, 7957 (2015).
14. T. W. Hänsch, "Nobel lecture: passion for precision," Rev. Mod. Phys. **78**, 1297–1309 (2006).
15. J. Liu, A. S. Raja, M. Karpov, *et al.*, "Ultralow-power chip-based soliton microcombs for photonic integration," Optica **5**, 1347–1353 (2018).
16. P. Del'Haye, S. A. Diddams, and S. B. Papp, "Laser-machined ultra-high-Q microrod resonators for nonlinear optics," Appl. Phys. Lett. **102**, 221119 (2013).
17. S. H. Lee, D. Y. Oh, Q.-F. Yang, *et al.*, "Towards visible soliton microcomb generation," Nat. Commun. **8**, 1295 (2017).
18. G. Frigenti, D. Farnesi, G. Nunzi Conti, *et al.*, "Nonlinear optics in microspherical resonators," Micromachines **11**, 303 (2020).
19. D.-Q. Yang, J.-H. Chen, Q.-T. Cao, *et al.*, "Operando monitoring transition dynamics of responsive polymer using optofluidic microcavities," Light Sci. Appl. **10**, 128 (2021).
20. N. Toropov, G. Cabello, M. P. Serrano, *et al.*, "Review of biosensing with whispering-gallery mode lasers," Light Sci. Appl. **10**, 42 (2021).
21. X. Jiang, A. J. Qavi, S. H. Huang, *et al.*, "Whispering-gallery sensors," Matter **3**, 371–392 (2020).
22. H. Yang, Z.-G. Hu, Y. Lei, *et al.*, "High-sensitivity air-coupled megahertz-frequency ultrasound detection using on-chip microcavities," Phys. Rev. Appl. **18**, 034035 (2022).
23. S. A. Diddams, T. Udem, J. Bergquist, *et al.*, "An optical clock based on a single trapped $^{199}Hg^{+}$ ion," Science **293**, 825–828 (2001).
24. Z. L. Newman, V. Maurice, T. Drake, *et al.*, "Architecture for the photonic integration of an optical atomic clock," Optica **6**, 680–685 (2019).
25. M.-G. Suh, Q.-F. Yang, K. Y. Yang, *et al.*, "Microresonator soliton dual-comb spectroscopy," Science **354**, 600–603 (2016).
26. P. Trocha, M. Karpov, D. Ganin, *et al.*, "Ultrafast optical ranging using microresonator soliton frequency combs," Science **359**, 887–891 (2018).
27. J. Riemensberger, A. Lukashchuk, M. Karpov, *et al.*, "Massively parallel coherent laser ranging using a soliton microcomb," Nature **581**, 164–170 (2020).
28. J. Pfeifle, V. Brasch, M. Lauermann, *et al.*, "Coherent terabit communications with microresonator Kerr frequency combs," Nat. Photonics **8**, 375–380 (2014).
29. J. Pfeifle, A. Coillet, R. Henriet, *et al.*, "Optimally coherent Kerr combs generated with crystalline whispering gallery mode resonators for ultrahigh capacity fiber communications," Phys. Rev. Lett. **114**, 093902 (2015).
30. P. Marin-Palomo, J. N. Kemal, M. Karpov, *et al.*, "Microresonator-based solitons for massively parallel coherent optical communications," Nature **546**, 274–279 (2017).
31. Y. Geng, H. Zhou, X. Han, *et al.*, "Coherent optical communications using coherence-cloned Kerr soliton microcombs," Nat. Commun. **13**, 1070 (2022).

32. T. Salgals, J. Alnis, R. Murnieks, *et al.*, "Demonstration of a fiber optical communication system employing a silica microsphere-based OFC source," Opt. Express **29**, 10903–10913 (2021).
33. Z. Zhou, J. Wei, Y. Luo, *et al.*, "Communications with guaranteed bandwidth and low latency using frequency-referenced multiplexing," Nat. Electron. **6**, 694–702 (2023).
34. A. B. Matsko and L. Maleki, "On timing jitter of mode locked Kerr frequency combs," Opt. Express **21**, 28862–28876 (2013).
35. F. Lei, Z. Ye, Ó. B. Helgason, *et al.*, "Optical linewidth of soliton microcombs," Nat. Commun. **13**, 3161 (2022).
36. D. Zou, Y. Chen, F. Li, *et al.*, "Comparison of bit-loading DMT and pre-equalized DFT-spread DMT for 2-km optical interconnect system," J. Lightwave Technol. **37**, 2194–2200 (2019).
37. W. Wang, Z. Wu, D. Zou, *et al.*, "Training sequences design for simultaneously transceiver IQ skew estimation in coherent systems," J. Lightwave Technol. **42**, 5088–5098 (2024).
38. X. Yi, Q.-F. Yang, X. Zhang, *et al.*, "Single-mode dispersive waves and soliton microcomb dynamics," Nat. Commun. **8**, 14869 (2017).
39. T. Okoshi, K. Kikuchi, and A. Nakayama, "Novel method for high resolution measurement of laser output spectrum," Electron. Lett. **16**, 630–631 (1980).
40. T. Mukaihara, T. Kimura, and H. Koshi, "Narrow linewidth tunable lasers for digital coherent system," in *Conference on Lasers and Electro-Optics Pacific Rim* (Optica Publishing Group, 2015), paper 27J1_1.